Arabian Journal of Chemical and Environmental Researches Vol. 02 Issue 2 (2015) 37–50



Potentiodynamic polarization behavior of some austenitic stainless steel AISI samples of different molybdenum contents in H₂SO₄ solutions

M.A.M. Ibrahim^{1,2}*, S.S. Abd El Rehim² and M.M. Hamza²

¹Chemistry Department, Faculty of Science, Taibah University, 30002, Al Madina Al AlMounwara, KSA

²Chemistry Department, Faculty of Science, Ain Shams University, 11566 Abbassia, Cairo, Egypt

Received 29 Sept 2015, Revised 20 Oct 2015, Accepted 21 Oct 2015

Abstract

Potentiodynamic polarization behavior of some Egyptian austentic stainless steel; SS 304L (I), SS 304H (II), and SS 316H (III) of different Mo content was investigated in H₂SO₄ solutions. The study includes the effect of H₂SO₄ concentrations, scan rate and the temperature. The values of E_{corr} for each alloy sample is shifted greatly to more positive direction with increasing the acid concentration. Moreover, the value of j_{corr}, enhances with acid concentration for the three alloys. At a given acid concentration, the value of j_{corr}, and hence the corrosion rate of each alloy decreases in the following order:Alloy III > Alloy I. This means that the higher the Mo content in the alloy, the higher the corrosion rate. In addition, the rate of corrosion of each sample enhances with increasing the temperature as well as with increasing the scan rate.

Keywords: Stainless steel; H₂SO₄; potentiodynamic polarization curves; scan rate.

*Corresponding author.

E-mail address: imagdy1963@hotmail.com

1. Introduction

The austenitic stainless steels AISI have excellent corrosion resistance, very good formability, and show an increase in strength as a result of cold work; most are readily weldable. They also show good ductility and toughness even at high strengths, and these properties are retained down to cryogenic temperatures. In structural applications, the toughness and fatigue strength of these steels are important [1]. Because of their good mechanical properties and ease of fabrication, austenitic stainless steels are much more widely used than ferritic stainless steels. The high corrosion resistance of the stainless steel is attributable tothe presence of passive film [2]. This film is stable, invisible, thin, durable and extremely adherent and self-repairing. The stability of passive films and the reactions taking place in the transpassive potential region depend on the nature of the anode potential and the anion present.

The role played by the Mo content on the corrosion resistance of the stainless steel has not yet clearly established. In addition, the effect of molybdenum content on the corrosion resistance of stainless steel is greatly depend upon the type of the steel whether it is ferritic or austenitic[3] as well as on the nature of the corrosive medium. Although austenitic stainless steels exhibit a very high corrosion resistance over a broad range of conditions, they are not immune to every environment [4]. Sulphuric acid is very corrosive for stainless steels [5,6] and constitute one of the basic raw materials encountered in the chemical industry. The AISI of the types 304 and 316 are used to handle very diluted acid at low temperature [7]. In addition, in producing the acids, the problem of corrosion is significant in the production plants. The acid also causes major problem in consumers' plants when it is utilized under a wide variety of conditions. The corrosion resistance of austenitic stainless steels to sulphuric acid is a complicated process due to the active-passive nature of the alloys.

Therefore, the aim of this work was to evaluate the difference in potentiodynamic polarization behavior of SS 304L, SS 304H, and SS 316H, which have different molybdenum content, in sulphuric acid environments. In addition, the effect of temperature as well as the scan rate were investigated.

2. Experimental details

The austentic stainless steel; SS 304L (I), SS 304H (II), and SS 316H (III)SS 304L, SS 304H, and SS 316Halloy samples used in the present work were produced in the induction furnace of the Modern Foundries Company, Giza, Egypt. The working electrode was in the form of rod (5 mm diameter) and was embedded in a Pyrex glass tube sealed with Araldite to offer an exposed surface area of 0.28 cm². The chemical composition of these alloys and their abbreviations are given in Table 1.

Alloy symbol \mathbf{C} Si Mn \mathbf{Cr} Mo Cu Alloy Ni SS 304L (0.09 Mo) 0.031 2.180 0.033 0.330 1.900 18.01 8.11 0.09 0.004 II SS 304H (1.15 Mo) 0.220 1.250 1.200 19.45 9.45 1.15 0.025 0.015 0.200 III SS 316H (2.00 Mo) 0.200 1.130 1.250 18.35 8.80 **2.0**0 0.028 0.008 0.240

Table 1: Chemical composition (wt %) of the austenitic stainless-steel alloys

The electrode was polished with a series of emery papers, from a coarse one 500 and proceeding in steps to fine grade 1500, washed thoroughly with doubly distilled water, and then introduced into the test solution. A platinum wire was used as a counter electrode. All potentials were measured against a saturated calomel electrode. The measurements were carried out in three-electrode cell by using a computer-assisted Potentiostat ACM. The cell was placed in a water thermostat to attain the required temperature ±1.0°C. To investigate the effect of temperature, experiments were carried out at temperature range 10-75°C. All solutions were freshly prepared from analytical grade chemicals and doubly distilled water. The aqueous corrosion behavior of the samples was studied by using potentiodynamic polarization technique. The potentiodynamic polarization curves were recorded by sweeping the potential from the starting negative potential towards more positive direction with scan rate of 10 mVs⁻¹. To study the effect of scan rate on the polarization behaviors of the different stainless-steel alloys, the experiments were performed at sex scan rates of 5, 10, 20, 30, 50 and 100 mVs⁻¹. In all cases, duplicate experiments were carried out to ensure reproducibility.

3. Results and discussion

3.1. Effect of sulphuric acid concentrations:

Figures 1-3 depict the Tafel plots of AISI samples; I (SS 304L 0.09 Mo), II (SS 304H1.15 Mo) and III (SS 316H 2.00 Mo) respectively in various concentrations (0.05 - 1.00M) of H₂SO₄ at 25°C. The curves were swept from negative potential, where, hydrogen evolution reaction is the dominant, towards more positive potentials at a scan rate of 10 mVs⁻¹. It is observed that, in all cases, the polarization profiles have the same general feature. On positive going scan, the cathodic current density corresponding to hydrogen evolution reaction decreases gradually and changes its sign at zero current-potential. Around the zero current-potential, each curve exhibits Tafel behavior. The electrochemical parameters, the corrosion current, j_{corr} and the corrosion potential, E_{corr} were obtained by extrapolation of Tafel lines at various acid concentrations, and are given in Table 2.In addition, the anodic and cathodic Tafel slopes of these lines, $β_a$ and $β_c$ were found to be constant ($β_a$ = 707

mV/decade and β_c = 791 mV/decade) at all the H₂SO₄ concentration range used. The invariance in these values means that the dissolution mechanism is the same. It is clear that the values of E_{corr} for each alloy sample is shifted greatly to more positive direction with increasing the acid concentration. It is also found that, the value of j_{corr} of each sample, and hence its corrosion rate in H₂SO₄ solutions, is strongly depend on the acid concentration as well as on the alloy composition. Figure 4 illustrates the dependence of j_{corr} on log C_{acid}. It is clear that the value of j_{corr}, enhances with acid concentration for the three alloys, indicating that the SO₄²-ions participate directly in the corrosion events. On the other hand, careful examination of the data collected in Table 2, show that at a given acid concentration, the value of j_{corr}, and hence the corrosion rate of each sample decreases in the following order:

Alloy III > Alloy II> Alloy I

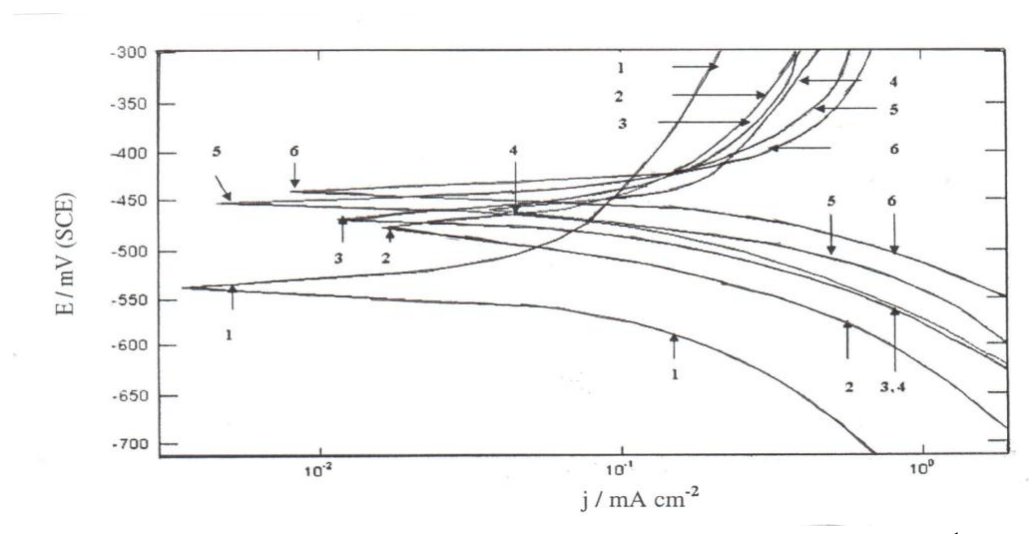


Fig. 1 Tafel plots of Alloy I in H₂SO₄ solutions of various concentrations at a scan rate of 10 mVs⁻¹ at 20°C(1) 0.05 M; (2)0.10 M; (3) 0.25M; (4) 0.50M and (5) 1.0M H₂SO₄

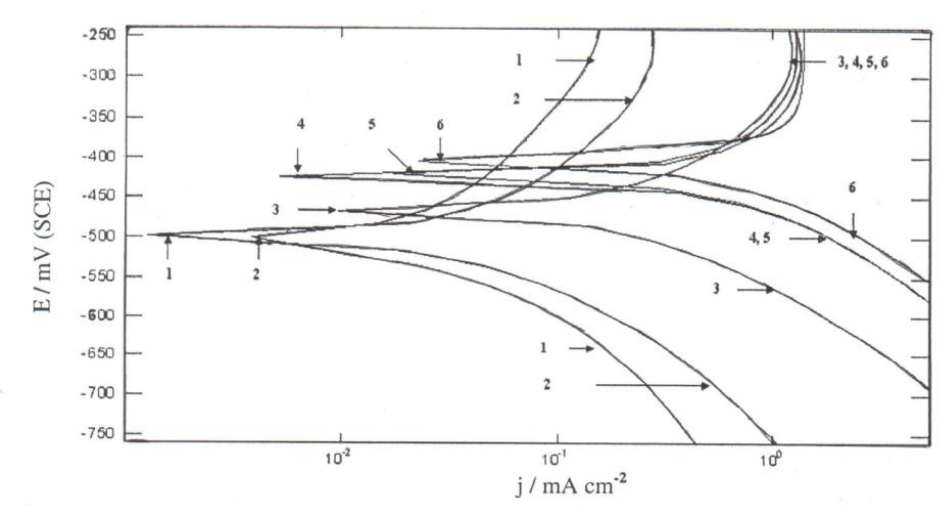


Fig. 2 Tafel plots of Alloy II in H_2SO_4 solutions of various concentrations at a scan rate of 10 mVs⁻¹ at 20°C (1) 0.05 M; (2) 0.10 M; (3) 0.25M; (4) 0.50M; (5) 0.75M and (6) 1.0M H_2SO_4 .

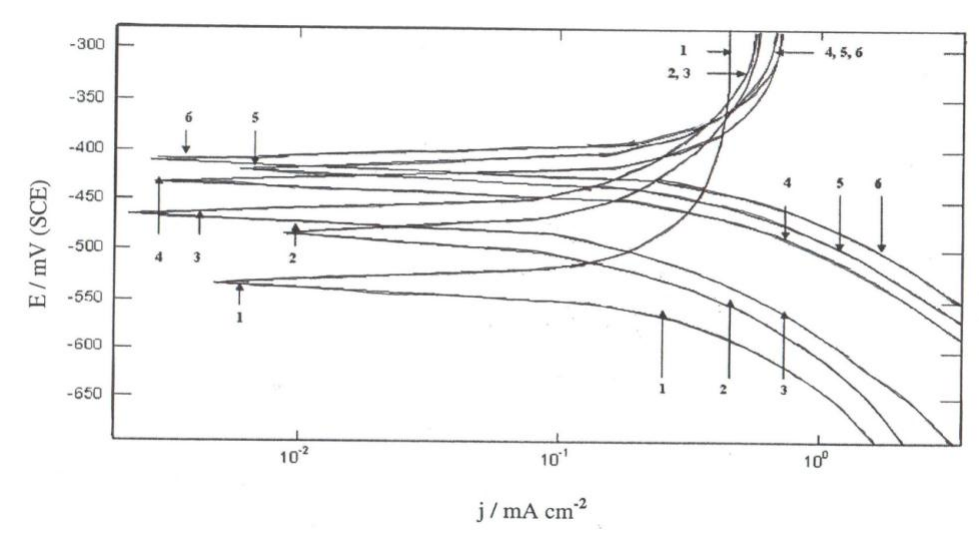


Fig. 3 Tafel plots of Alloy III in H_2SO_4 solutions of various concentrations at a scan rate of 10 mVs⁻¹ at 20°C (1) 0.05 M; (2) 0.10 M; (3) 0.25M; (4) 0.50M; (5) 0.75M; and (6) 1.0M H_2SO_4 .

Table 2. Electrochemical parameters E_{corr}, and j_{corr}, associated with polarization measurements recorded for alloys I, II and III in various concentrations of H₂SO₄ at 25° C.

Conc.	All	oy I	Allo	y II	Alloy III				
H ₂ SO ₄ /	-E _{corr}	$j_{ m corr}$	-E _{corr}	r j _{corr} -E _{corr}		jcorr			
M	(mV)	(mA cm ⁻²)	(mV)	(mA cm ⁻²)	(mV)	(mA cm ⁻²)			
0.05	537	0.814	500	1.90	540	2.53			
0.10	475	4.260	496	4.90	490	5.90			
0.25	468	12.57	467	27.03	466	13.20			
0.50	460	22.28	420	53.52	427	65.37			
0.75	455	22.40	422	66.26	420	72.25			
1.00	442	22.68	403	85.20	412	86.76			

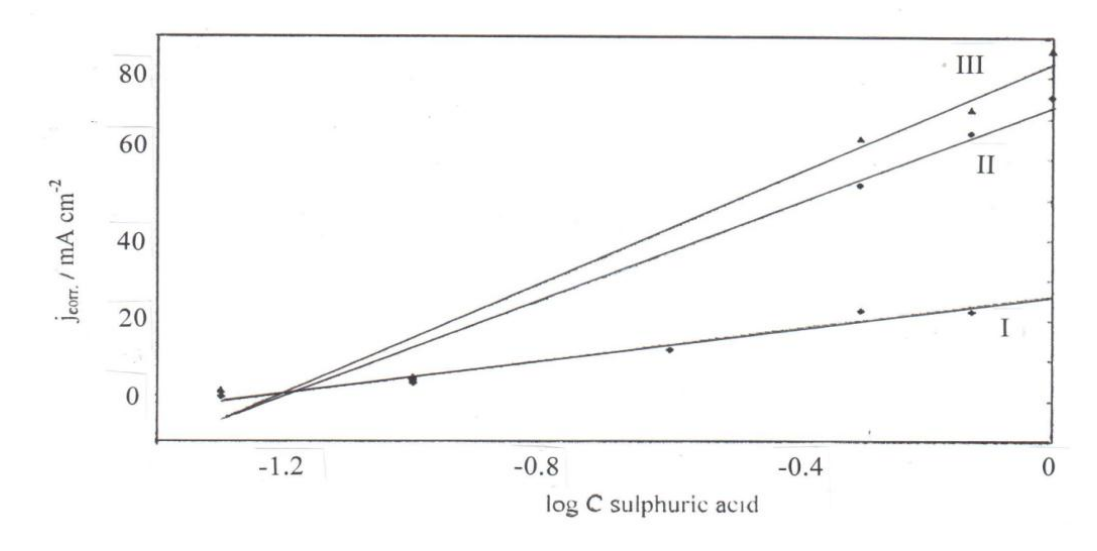


Fig. 4 The relation between current density (j_{corr}) and $log\ C_{acid}$ for Alloys I, II and III in H_2SO_4 solution of various concentrations at $25^{\circ}C$.

Such trend could be related to the Mo content in the alloy. According to our previous study [8] with the same AISI alloy samples in NaCl solution, it was found that the higher the Mo content in the alloy, the lower is the value of j_{corr} and consequently the corrosion rate. In contrast, in the present study in H₂SO₄, it is found that the higher the Mo content in the alloy, the higher the value of j_{corr}. This means that the beneficial effect of Mo content in the alloys observed in NaCl medium does not appear in sulfuric acid solutions. The simulation effect is due to dissolution of Mo of corroding alloys to generate Mo³⁺ and / or Mo⁵⁺ soluble species in H₂SO₄ solution. Both Mo³⁺ and / or Mo⁵⁺ did not exert inhibition effect on corrosion process [9]. Therefore, one can conclude that the dissolution of Mo content of the corroding alloys is the reason for the acceleration of corrosion.

On the other hand, the anodic excursions of the polarization profiles (Figs 5-7) are characterized by the appearance of active-passive-transpassive behavior before oxygen evolution potential.

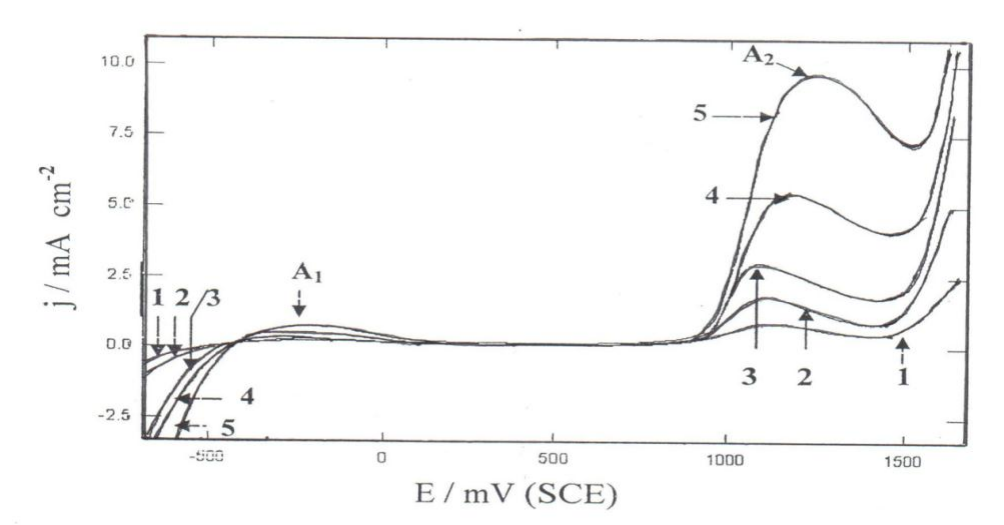


Fig. 5 Potentiodynamic anodic polarization curves for Alloy I in H₂SO₄ solutions of various concentrations at a scan rate of 10 mV s⁻¹ and at 25°C (1) 0.05; (2) 0.10M; (3) 0.25M; (4) 0.50M and (5) 1.0M H₂SO₄.

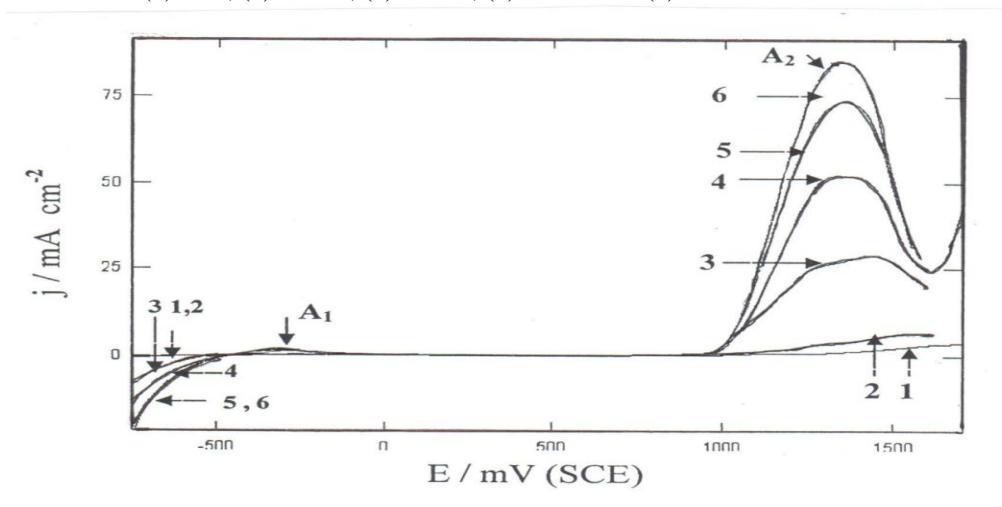


Fig. 6 Potentiodynamic anodic polarization curves for Alloy II in H₂SO₄ solutions of various concentrations at a scan rate of 10 mV s⁻¹ and at 25°C (1) 0.05; (2) 0.10M; (3) 0.25M; (4) 0.50M; (5) 0.75M and (5) 1.0M H₂SO₄.

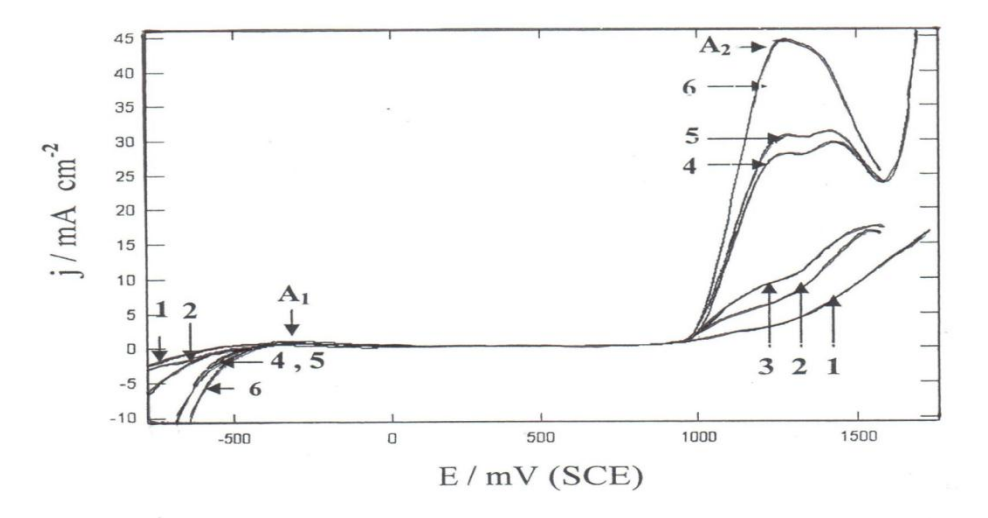


Fig. 7 Potentiodynamic anodic polarization curves for Alloy III in H₂SO₄ solutions of various concentrations at a scan rate of 10 mV s-1 and at 25oC (1) 0.05; (2) 0.10M; (3) 0.25M; (4) 0.50M; (5) 0.75M and (5) 1.0M H₂SO₄.

The appearance of the active anodic dissolution region, peak A1,is due to iron dissolution from the alloy surface as Fe²⁺. Wanklyn [10] suggested that both Mo³⁺ and Mo⁵⁺ can be generated from Mo content of an alloy in active anodic dissolution potential region (peak A₁ region). As can be seen, the potentiodynamic polarization curves are characterized by a very wide potential domain of passivity (≈ 500 mV in case of alloy I and ≈ 1000 mV in case of alloy II and III). The peak current density, j_{A1}, for each sample increases with increasing acid concentration. Figure 8 depicts the relation between, j_{A1} and log C_{acid} concentration. It is found that at each acid concentration, the peak current density, j_{A1}, increases with increasing Mo content of the samples, as a result of dissolution of Mo and formation of soluble species of Mo³⁺ and Mo⁵⁺.

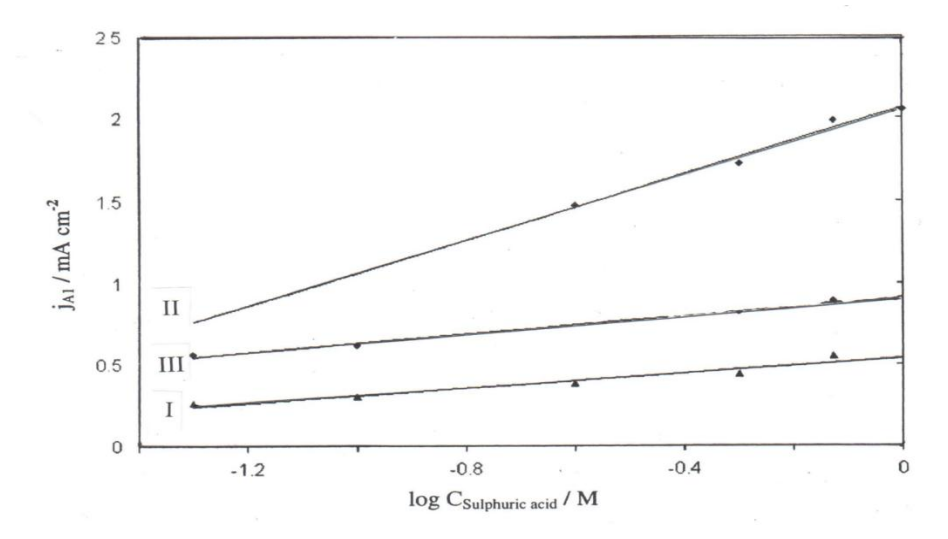


Fig. 8 Relation between log C_{acid} and current density of peak A_1 (j_{A1}) of active dissolution of Alloys I, II and III in various concentrations of H_2SO_4 at a scan rate of 10 mV s⁻¹ and at 25°C.

When the active dissolution current density reaches its maximum value, j_{A1}, the anodic current density decreases rapidly to a very small value of passive current, jpass. Passivity of the alloy is due to the formation of iron oxide and chromium oxide on the sample surface [11]. In case of NaCl solution [8], the potentiodynamic polarization curves do not exhibit active-passive transition. However, it exhibited a wide potential domain of passivity up to a certain critical potential, pitting potential, Epit, at which the small passive current density increases rapidly without any sign for oxygen evolution, which indicating initiation of pitting corrosion. However, in H₂SO₄ solution, the passive region is limited by the appearance of transpassive dissolution region, peak A₂ (Figs. 5-7). Transpassive dissolution of metals and alloys at high anodic potentials can be related to electrochemical reactions in the solid-state involving transition to higher oxidation state than that in the passive state. In many cases, the produced species are soluble and go in the solution resulting, therefore, in the appearance of transpassive dissolution region [10]. The relative dissolution of Fe in the alloys makes the surface rich in Cr and Mo. Therefore, one can suggest that the transpassive dissolution peak, A₂, for the three samples is due to the oxidation of Cr³⁺ to Cr⁶⁺ within the passive film and the formation of soluble $\text{CrO}_4^{2^-}$ ions [12,13]. Mo also dissolves in this high potential range as Mo^{6^+} [HMoO₄ $^-$ or MoO₄ 2 -] instead of Mo³⁺ and Mo⁵⁺ [10]. The dependence of the peak current density of peak A₂ on log C_{acid} for the three alloys is shown in Figure 9. It is clear that j_{A2} increases with increasing acid concentration. However, at a given acid concentration, the value of j_{A2} decreases with increasing Mo content in the alloys. Such beneficial effect of Mo could be explained on the basis that the molybdate [HMoO₄⁻ and / or MoO₄²⁻] anions act as inhibitors [10]. Theses anions can adsorb on the anode surface and form a barrier membrane upon it and inhibit transpassive dissolution. Moreover, these anions can repair the damaged oxide film upon the surface and therefore increases its protectiveness [11].

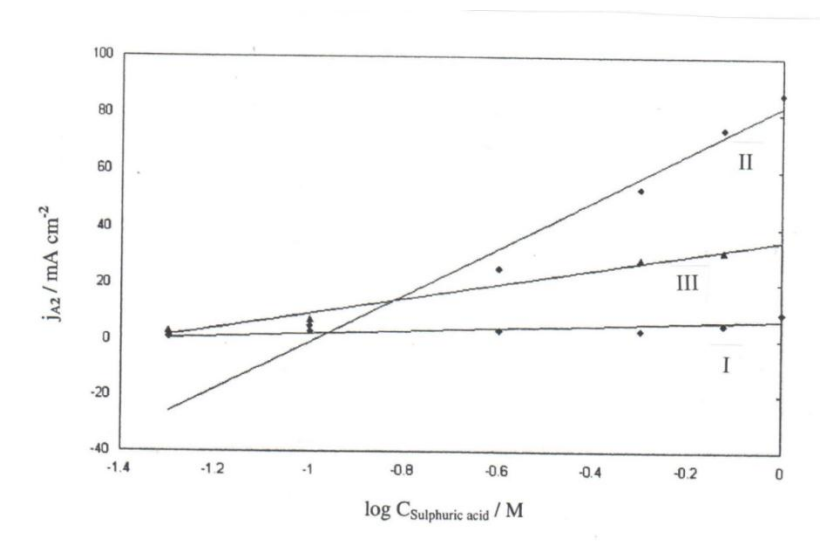


Fig. 9 Relation between log C_{acid} and current density of peak A_2 (j_{A2}) of active dissolution of Alloys I, II and III in various concentrations of H_2SO_4 at a scan rate of 10 mV s⁻¹ and at 25°C.

3.2. Effect of temperature:

Figures 10-12 show the effect of temperature (10-75°C) on Tafel plots of alloys I, II and III in 0.5 M H₂SO₄ respectively. The temperature favors the cathodic reaction and more specifically, it favors the hydrogen evolution reaction (HER) which leads to an increase of H₂evolution. On other words, an increase of temperature decreases the cathodic overpotential as a result of decreasing the activation overpotential of hydrogen evolution reaction. Moreover, temperature also favors the kinetics of the corrosion reactions, and especially the anodic dissolution of the alloy, since the corrosion current densities are high for each alloy as temperature increases (Table 3). The kinetic parameters associated with polarization curves were obtained and are given in Table 3 for alloys I, II and III.

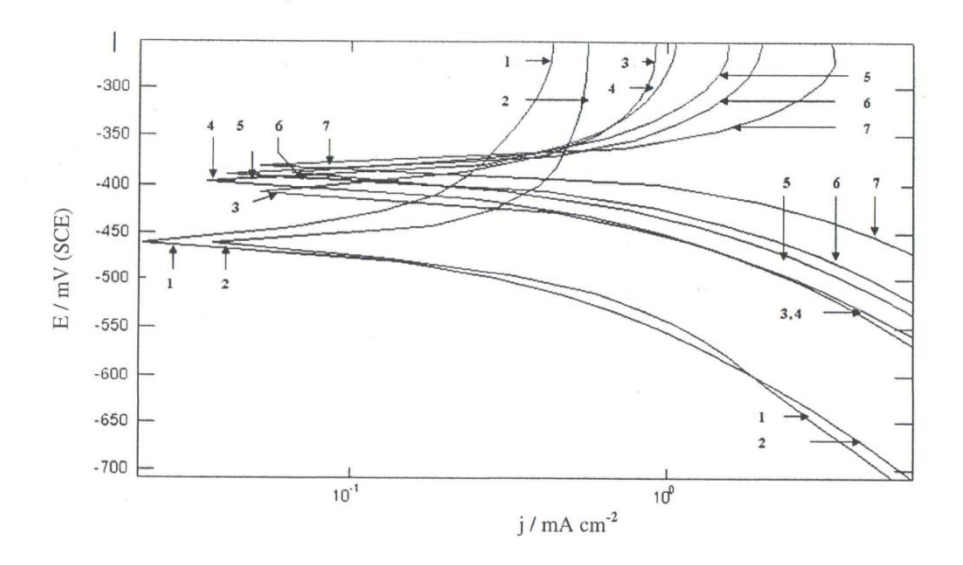


Fig. 10 Tafel plots of Alloy I in H_2SO_4 solutions of various concentrations at different temperatures:(1) $10^{\circ}C$; (2) $25^{\circ}C$; (3) $35^{\circ}C$; (4) $45^{\circ}C$; (5) $55^{\circ}C$ (6) $65^{\circ}C$ and (7) $75^{\circ}C$.

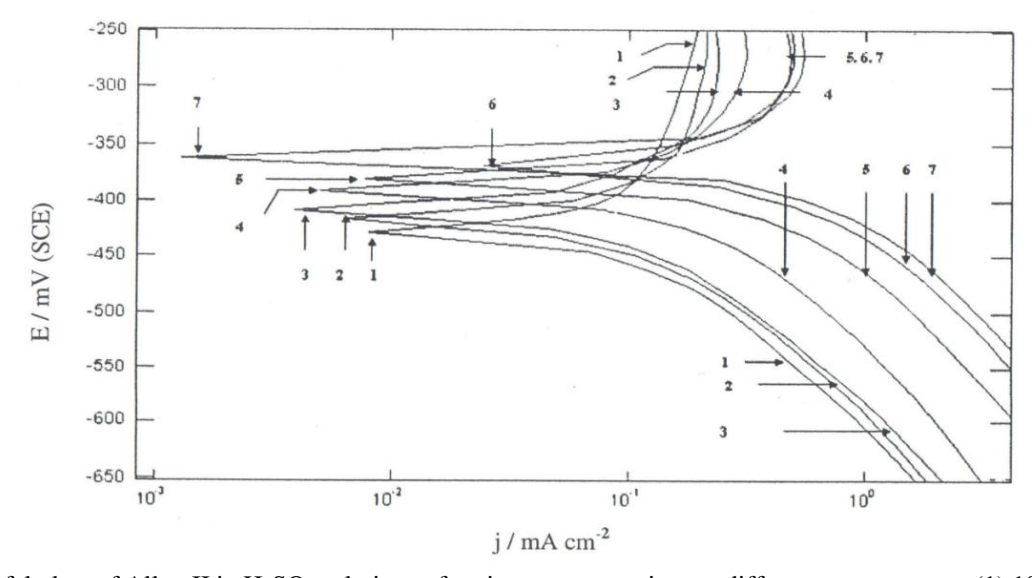


Fig. 11 Tafel plots of Alloy II in H_2SO_4 solutions of various concentrations at different temperatures: (1) $10^{\circ}C$; (2) $25^{\circ}C$; (3) $35^{\circ}C$; (4) $45^{\circ}C$; (5) $55^{\circ}C$ (6) $65^{\circ}C$ and (7) $75^{\circ}C$.

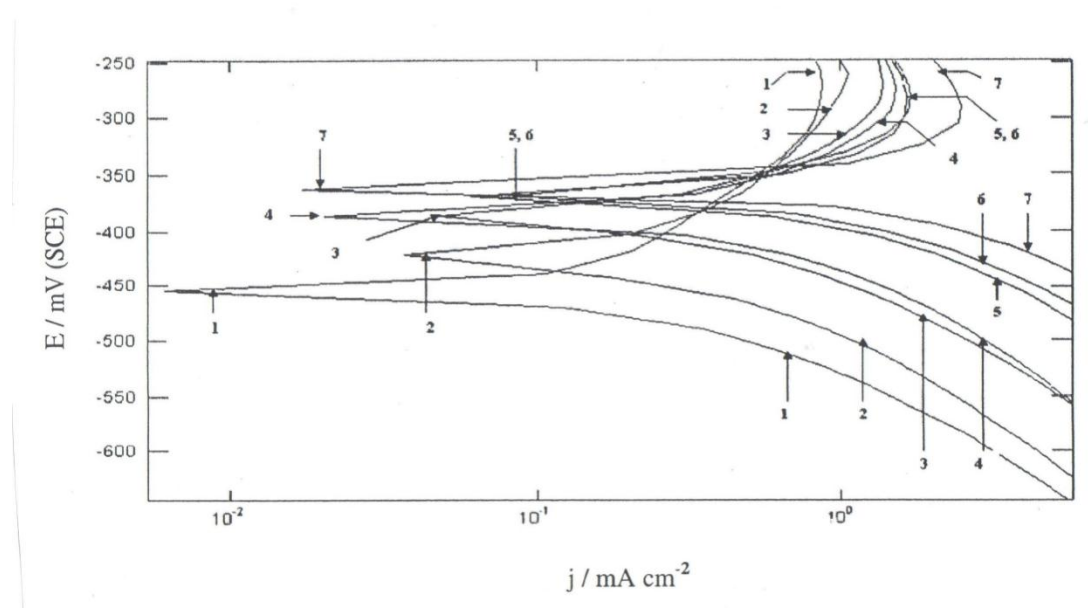


Fig. 12 Tafel plots of Alloy III in H_2SO_4 solutions of various concentrations at different temperatures: (1) $10^{\circ}C$; (2) $25^{\circ}C$; (3) $35^{\circ}C$; (4) $45^{\circ}C$; (5) $55^{\circ}C$ (6) $65^{\circ}C$ and (7) $75^{\circ}C$.

Table 3 Electrochemical parameters E_{corr} , and j_{corr} , associated with polarization measurements recorded for alloys I, II and III in 0.5 M H_2SO_4 at different temperatures.

Temp./°C	j c	orr (mA cm	2)	-E _{corr} (mV)			
	Alloy I	Alloy II	Alloy III	Alloy I	Alloy II	Alloy III	
10	18.21	45.85	47.75	460	440	455	
25	22.28	53.52	65.37	460	420	427	
35	22.30	64.28	76.50	407	407	386	
45	22.64	65.00	78.10	396	390	385	
55	24.57	67.00	80.58	388	380	377	
65	32.00	70.88	112.5	388	366	368	
75	34.13	71.16	113.9	383	360	363	

The values of j_{A1}, j_{pass} and j_{A2} increase with rising temperature. It is seen that an increase in temperature retards passivation and shifts the peak potential of peak A₁ to more positive direction (Figures 13-15). The increase in, j_{pass}, could be interpreted on the basis that an increase in temperature increases the porosity of the passive film and makes some intrinsic modifications in its chemical and / or physical structure [14]. Moreover, these modifications in the structure of the passive film may assist the transpassive dissolution. Also, the increase of temperature may weaken the adsorption strength of molybdate anions on the anode surface within transpassive region, and therefore decreases their inhibition action. Also, investigation of the data in Figs 13-15 show that the increase of temperature effects on the passivity range of the alloy. As a consequence, the abrupt increase of current density, which indicates the loss of passivity, occurs at lower potentials as temperature increases (Table 3).

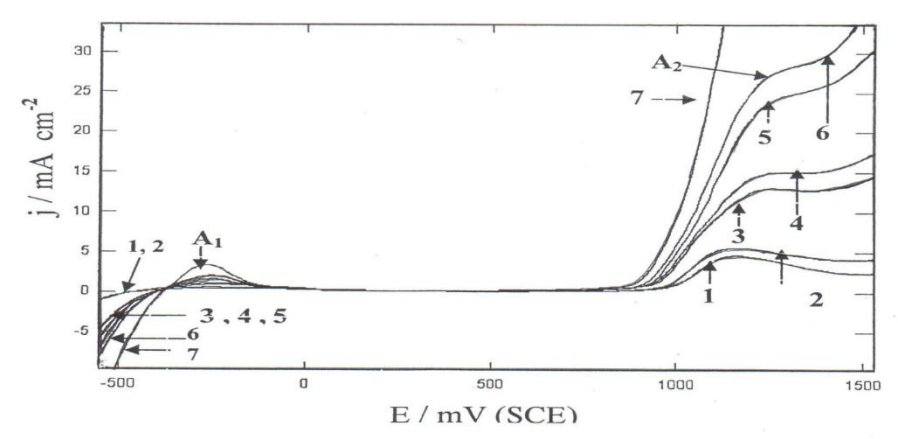


Fig. 13 Potentiodynamic anodic polarization curves for Alloy I in 0.50M H2SO4 solution at a scan rate 10 mVs⁻¹ and at different temperatures: (1)10°C; (2) 25°C; (3) 35°C; (4)45°C; (5) 55°C (6) 65°C and (7) 75°C.

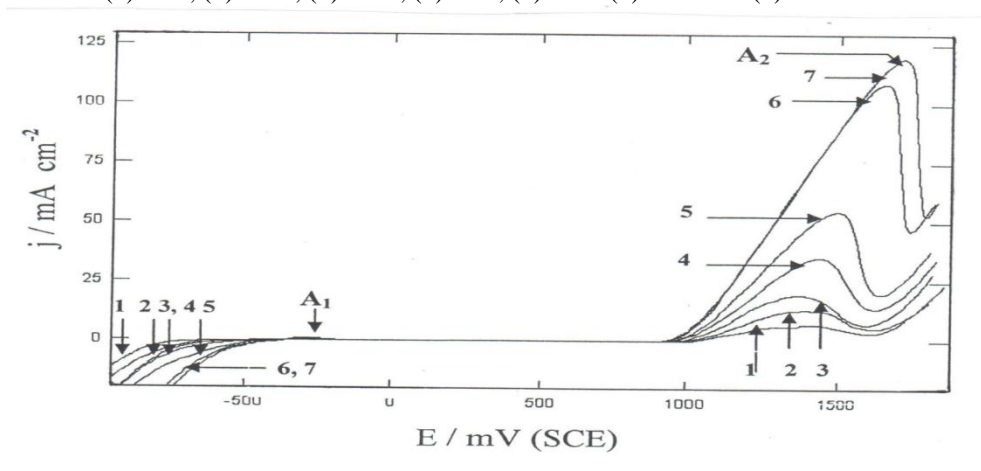


Fig. 14 Potentiodynamic anodic polarization curves for Alloy II in 0.50M H2SO4 solution at a scan rate 10 mVs⁻¹ and at different temperatures: (1) 10°C; (2) 25°C; (3) 35°C; (4)45°C; (5) 55°C (6) 65°C and (7) 75°C.

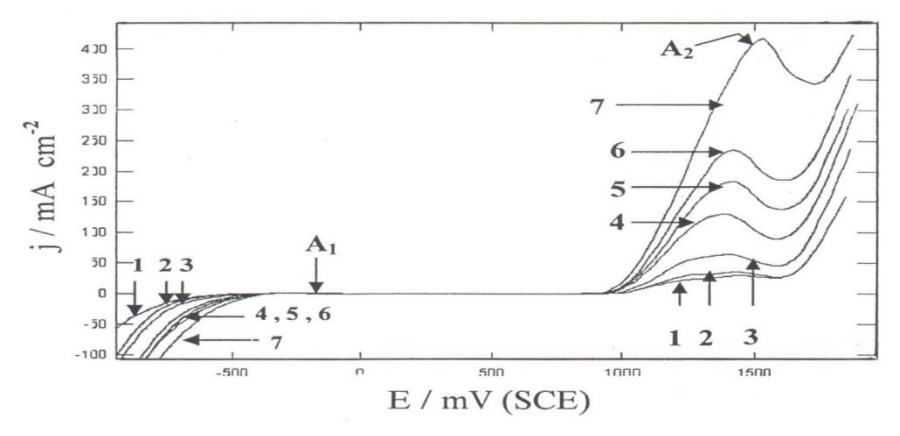


Fig. 15 Potentiodynamic anodic polarization curves for Alloy III in 0.50M H2SO4 solution at a scan rate 10 mVs⁻¹ and at different temperatures: (1) 10°C; (2) 25°C; (3) 35°C; (4)45°C; (5) 55°C (6) 65°C and (7) 75°C.

3.3. Effect of scan rate:

The influence of the potential scan rate, v, $(5.00 - 100 \text{ mVs}^{-1})$ on the potentiodynamic polarization curves of the three alloys in $0.5 \text{ M H}_2\text{SO}_4$ solution at 25°C were studied (curves are not included). The corrosion potential, E_{corr} and the corrosion current j_{corr} were obtained by extrapolation of anodic and cathodic Tafel lines to the point of intersection. The obtained values are given in Table 4. The

values of j_{A1} and j_{A2} were also obtained from their corresponding curves and their values are included in Table 4.

Table 4 Electrochemical parameters (E_{corr} , j_{corr} , j_{A1} and j_{A2}) associated with polarization measurements recorded for
alloys I, II and III in 0.5 M H ₂ SO ₄ at different scan rates and at 25°C.

Scan	Alloy I			Alloy II				Alloy III				
rate	-E _{corr}	$j_{ m corr}$	j A1	j _{A2}	-E _{corr}	$j_{ m corr}$	j A1	j _{A2}	-E _{corr}	j_{corr}	j A1	j _{A2}
mV/s	(mV)	mA cm ⁻²	mA cm ⁻²	mA cm ⁻²	(mV)	mA cm ⁻²	mA cm ⁻²	mA cm ⁻²	(mV)	mA cm ⁻²	mA cm ⁻²	mA cm ⁻²
5	391	19.0	0.24	3.37	397	47.14	0.60	49.82	376	56.70	0.34	25.76
10	425	19.05	0.36	4.20	415	51.24	1.41	52.2	395	63.10	0.48	26.77
20	460	22.25	0.59	6.00	420	53.52	1.72	52.7	427	65.37	0.82	29.98
30	456	23.45	0.83	7.98	453	54.97	2.38	59.43	448	66.71	1.00	33.70
50	460	23.60	1.30	10.40	470	56.37	3.58	65.9	453	67.40	1.60	40.97
100	460	23.91	2.00	15.76	524	60.90	4.28	78.20	477	70.20	2.70	50.00

Inspection of the data reveals that an increase in the scan rate, υ , not only shifted the E_{corr} to more negative potential values but also increases, j_{corr} , and hence the rate of general corrosion of these alloys in H_2SO_4 . A similar behavior was observed in NaCl solution [15]. Moreover, an increase in υ accelerates the active and transpassive dissolution of these samples and shifts their peak potentials to more positive values. The influence of scan rate, υ , on peak current densities j_{A1} and j_{A2} is shown in Figures 16 and 17, whereby, j_{A1} and j_{A2} versus $\upsilon^{1/2}$ were plotted.

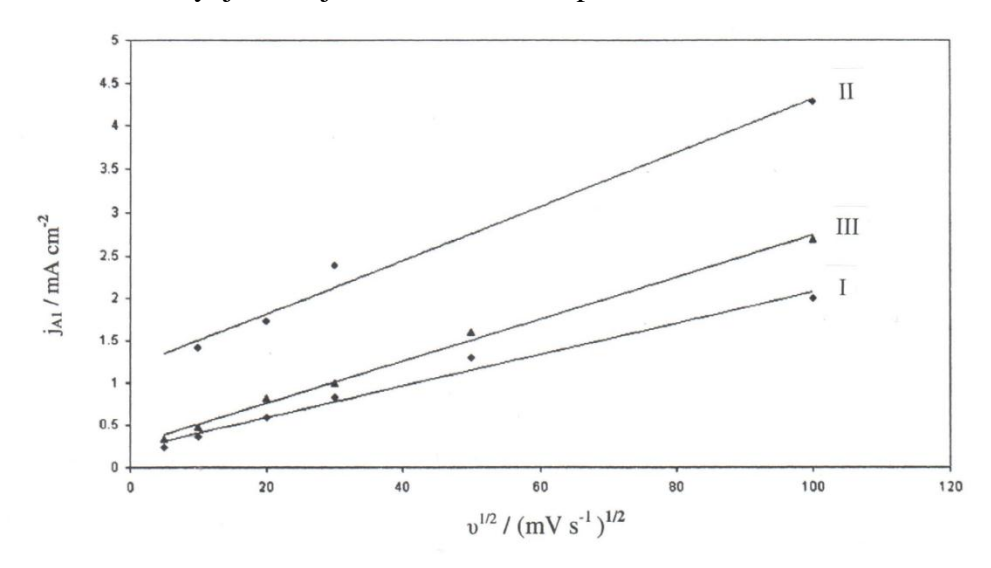


Fig. 16 Relation between current density of peak A1 (j_{A1}) and square root of scan rate $(v^{1/2})$ for Alloy I, II and III in 0.50M H_2SO_4 solution at 25°C.

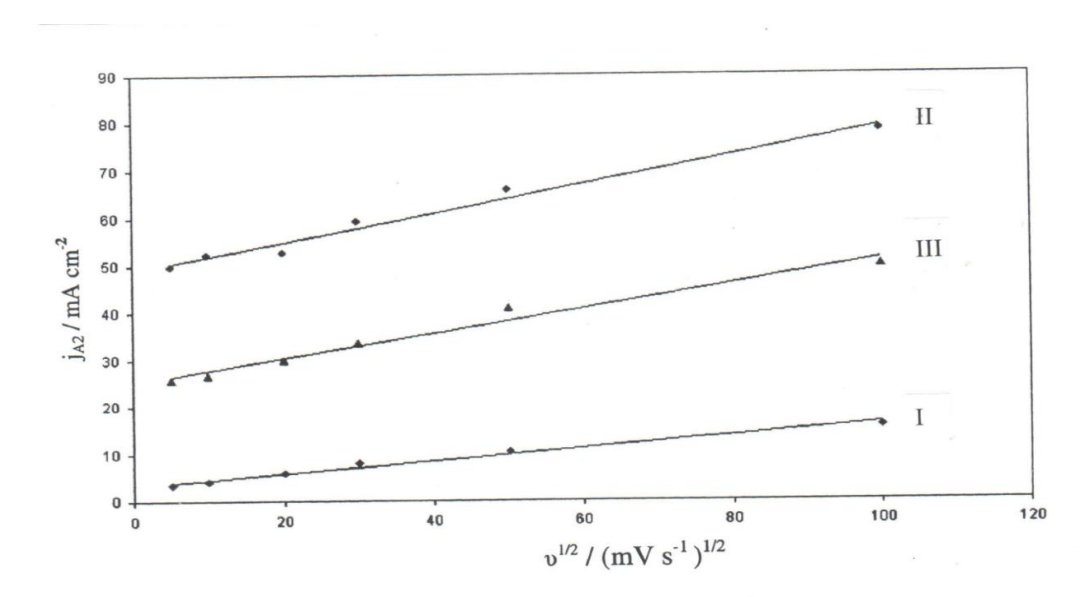


Fig. 17 Relation between current density of peak A2 (j_{A2}) and square root of scan rate ($v^{1/2}$) for Alloy I, II and III in 0.50M H₂SO₄ solution at 25°C.

Linear relationships are found, which indicate that the active and transpassive dissolution of the samples within the potential ranges of peaks A_1 and A_2 are, in principles, partially controlled by diffusion.

Conclusion

The corrosion behavior of some Egyptian austentic stainless steel; SS 304L (I), SS 304H (II), and SS 316H (III) of different Mo content was investigated in H₂SO₄ solutions using potentiodynamic polarization and the results obtained can be summarized as follows:

- (i) The potentiodynamic polarization curves are characterized by a very wide potential domain of passivity (≈ 500 mV in case of alloy I) and ≈ 1000 mV in case of alloy II and III).(
- (ii) The value of corrosion current of each sample, and hence its corrosion rate in H₂SO₄ solutions, is strongly depend on the acid concentration as well as on the alloy composition.
- (iii) At a given acid concentration, the value of corrosion current and hence the corrosion rate of each sample decreases in the following order:

Alloy III > Alloy II > Alloy I

(iv) An increase in the scan rate not only shifted the E_{corr} to more negative potential values but also increases, j_{corr} , and hence the rate of general corrosion of these alloys in H_2SO_4 .

References:

[1] R.W. Greene "The Chemical Engineering Guide to Corrosion", *McGraw-Hill Publications Co.*, New York, 1986.

- [2] J. Sedriks, Corrosion of Stainless Steels, 2nd ed., John Willey & Sons, Inc., New York, 1996.
- [3] M. G. S. Ferreira and J. L. Dawson, Electrochemical studies of the passive film on 316 stainless steel in chloride media, *J. Electrochem. Soc.*, 132, 760 (1995).
- [4] G.T. Burstein and B.T. daymond, The remarkable passivity of austenitic stainless steel in sulphuric acid solution and the effect of repetitive temperature cycling, *Corros. Sci.*, 51, 2249 (2009).
- [5] D. Jegdic, D.M. Drazic and J.P. Popic, Corrosion potential of 304 stainless steel in sulfuric acid (Preliminary communication), *J. Serb. Chem. Soc.*, 71(5), 543 (2006).
- [6] M. M. Hamza, S.S. Abd El Rehim, and M. A. M. Ibrahim, Inhibition effect of hexadecyl pyridinium bromide on the corrosion behavior of some austenitic stainless steels in H2SO4 solutions, *Arab. J. Chem.*, 6, 413 (2013).
- [7] H. Alves, D.C. Agarwal, H. Werner, *Nace-International Corrosion Conference Series*, 2006, Houston, 62221.
- [8] M. A. M. Ibrahim, S. S. Abd El Rehim, M.M. Hamza, Corrosion behavior of some austenitic stainless steels in chloride environments, *Mater. Chem. Phys.*, 115, 80 (2009).
- [9] H. H. Hassan, S. S. Abd El Rehim, N. F. Mohamed, Corros. Sci., 44, 37 (2002).
- [10] J. N. Wanklyn, Corros. Sci., 21, 211 (1981).
- [11] Z. Misirlioglu, S. Uneri and M. L. Aksu, Corrosion Behaviour of Mo and Mo Containing and Mo Free Steels in Basic and Acidic Media. *J. Corros. Sci. Engineering*, 3, 8 (2001).
- [12] Q. Yang and J.L. Luo, The hydrogen-enhanced effects of chloride ions on the passivity of type 304 stainless steel, *Electrochim. Acta*, 45, 3927(2000).
- [13] A. V. Alves and C.M. A. Brett, Characterisation of passive films formed on mild steels in bicarbonate solution by EIS, *Electrochim. Acta*, 47, 2081 (2002).
- [14] S. Nigshen, U. K. Mudali and R. K. Dayal, Electrolyte and temperature effects on pitting corrosion of type 316LN stainless steels, *Br. Corros. J.*, 36, 1 (2001).
- [15] Y. Yi, P. Cho, A. Al Zaabi, Y. Addad and C. Jang, Potentiodynamic polarization behaviour of AISI type 316 stainless steel in NaCl solution, *Corros. Sci.*, 74, 92 (2013).

(2015); www.mocedes.org/ajcer